CHAPTER IV

RESULTS AND DISCUSSION

4.1 Characterization of Fresh Catalysts

Table 4.1 shows properties of mono-, bi-, and trimetallic Pt-Sn-(RE) catalysts which were supported on the commercial KL zeolite. The rare earth (RE) elements investigated in this work are Thulium (Tm) and Cerium (Ce). The catalysts were prepared by vapor-phase impregnation method with different orders of impregnation.

**Table 4.1** Properties of mono-, bi-, and trimetallic Pt-Sn-(RE)/KL catalysts investigated in this work

Catalyst	wt% Pt	wt% Sn	wt% RE	Order of Impregnation
Pt/KL	1	0	0	Pt
Sn/KL	0	1	0	Sn
Tm/KL	0	0	0.15	Tm
Ce/KL	0	0	0.15	Ce
PtSn/KL	1	1	0	(Pt+Sn)
PtSn/Tm/KL	1	1	0.15	Tm, (Pt+Sn)
PtSn/Ce/KL	1	1	0.15	Ce, (Pt+Sn)

To determine the effect of promoters on the reducibility of catalysts, the Pt-Sn/KL and PtSnRE/KL catalysts were characterized by TPR technique. TPR experiments were carried out to investigate the reducibility of samples. Figure 4.1 shows the TPR profiles of the mono-, bi-, and trimetallic Pt-Sn-(RE) supported on commercial KL zeolite. For the monometallic, Pt/KL catalyst with a board reduction peak centered at ca. 180°C represented the reduction of Pt (IV) to Pt° (Ostgard *et al.*, 1992; Zheng *et al.*, 1996; and Rodriguez *et al.*, 2005). Moreover, the reduction temperature of Tm showed at 530°C while the profile of Ce in supported KL zeolite was not shown. In contrast, the TPR of Sn exhibited one broad reduction peak starting at 350°C with the maximum around 550°C (Trakarnroek *et al.*, 2007). When the pro-

files of both monometallic Pt and Sn catalysts were combined, the resulting profile did not match any profiles of the bimetallic PtSn/KL catalysts. Since the TPR profiles of the bimetallic PtSn/KL consisted of the broad peak which can be deconvoluted into three main peaks centered at 140°C, 255°C, and 480°C. These peaks correspond to Pt (IV) to Pt° (Pt rich phase), Pt-Sn alloy phase, and Sn° (Sn rich phase), respectively. For trimetallic catalysts, 0.15 wt% of Ce or Tm, were integrated with PtSn/KL, the TPR profiles can be also deconvoluted into four main peaks. The additional peak was Pt-RE alloy phase. From Figure 4.1, it indicated that alloy peaks of PtSn/RE/KL are broader than PtSn/KL. It might be due to the metal interaction of Pt-Sn and Pt-RE. In addition, it was observed that reduction temperatures of trimetallic catalysts shift to higher temperature because of the alloy phase of the third promoters but it was still in the range of reduction temperature at 500°C.

Table 4.2 Deconvolution of TPR profiles of PtSn/KL and PtSn/RE/KL catalysts

Catalysts	Area of each TPR temperature (%)			
	100-220°C Pt rich phase	180-320°C Alloy phase of Pt-Sn catalyst	250-470°C Alloy phase of PtRE catalyst	360-580°C Sn&RE rich phase
PtSn/KL	11.56	70.43	0	18.01
PtSn/Tm/KL	6.49	50.65	22.22	20.64
PtSn/Ce/KL	8.67	47.75	26.21	17.37
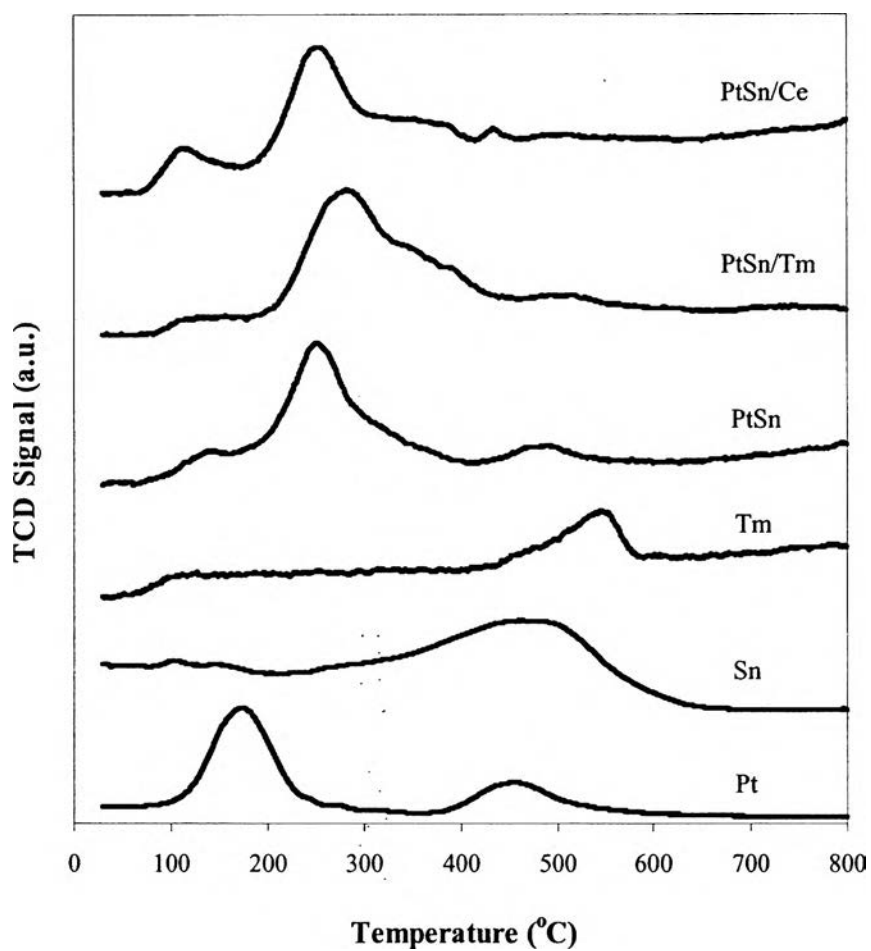
* TPR profile of Ce disappeared for supported KL zeolite.

Figure 4.1 TPR profiles of the mono-, bi-, and trimetallic Pt/KL, PtSn/KL, and PtSnRE/KL catalysts prepared by vapor-phase impregnation method.

Pt/KL   PtSn/KL
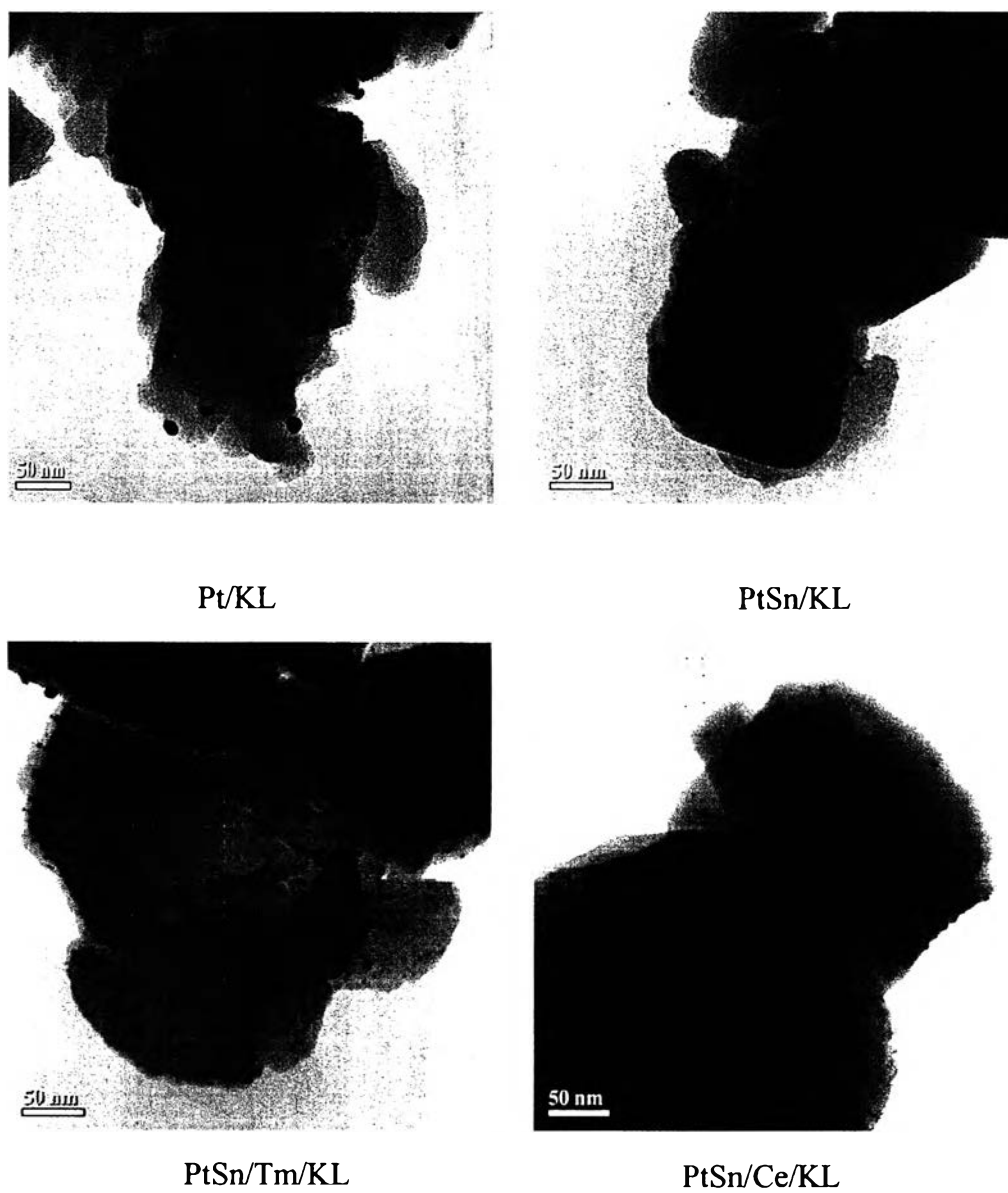
PtSn/Tm/KL   PtSn/Ce/KL

Figure 4.2 TEM images of particle size distribution obtained by TEM of the Pt/KL, PtSn/KL, and PtSn/RE/KL catalysts.

TEM images of particle size distribution obtained by TEM of the Pt/KL, PtSn/KL, and PtSn/RE/KL catalysts were depicted in Figure 4.2. Pt particles outside the zeolite were detected. The results showed that the addition of tin and rare earth elements enhanced the dispersion of metal and also decreased the particle size of metal compared with the unpromoted Pt/KL catalyst. The average particle size of the metal was reported in Table 4.3. It was found that the metal size was decreased to less than 2 nm for PtSn/KL and PtSn/Tm/KL catalysts, while there are some parts of metal clusters which have a larger particle size than 2 nm for such catalysts as observed in the histogram. However, the particles inside the pore of zeolite were not visible. TEM images are the evidence for external particles outside the pore of zeolite because of the limited performance of the TEM machine.

The results of hydrogen chemisorptions are listed in Table 4.3; the unpromoted Pt/KL catalyst exhibited higher H/Pt ratio than PtSn/KL and PtSn/RE/KL catalysts. The addition of tin and rare earth elements caused a strong decrease in the H/Pt ratio since Sn may partially cover the Pt resulting in low hydrogen adsorption (Passos et al., 1998).

Table 4.3 Analysis of fresh catalysts

Catalyst	wt% Pt	wt% Sn	wt% RE	H/Pt ratio after reduction at 500°C	Average metal size (nm) (measured from TEM)
Pt/KL	1	0	0	1.32	6.91-13.06
CoPtSn/KL	1	1	0	0.14	1.18-3.53
SeqPtSn/Tm/KL	1	1	0.15	0.14	1.29-6.45
SeqPtSn/Ce/KL	1	1	0.15	0.16	2.63-6.05

4.2 Catalytic Activity Testing: *n*-Octane Aromatization

4.2.1 Sulfur-free Feed

All catalysts were tested for *n*-octane aromatization at 500°C and atmospheric pressure. The variations of *n*-octane conversion with time on stream for the mono-, bi-, and trimetallic catalysts are illustrated in Figure 4.3 (a). It was found that Pt/KL exhibited a rapid deactivation due to coke plugging inside the pores because of the restricted diffusion out of the pore of C8-aromatic products (EB and OX) (Jongpatiwut *et al.*, 2005). Moreover, the presence of a promoter (Sn) caused a decrease in the initial activity due to the decrease in the platinum adsorption capacity as measured by hydrogen chemisorption. In a previous study, it was observed that the addition of the promoter such as tin improved the stability of the Pt/KL catalyst by inhibiting the adsorption of dehydrogenated species which is the intermediate for formation of coke (Hill *et al.*, 1998, Cortright *et al.*, 1994, 2000).

In terms of product selectivity, the results revealed that PtSn/KL and PtSn/RE/KL yield were higher selectivity to total aromatics and C8-aromatics selectivity than Pt/KL. Based on a previous study, it was found that the addition of Sn improved the stability of the Pt/KL catalyst by inhibiting the adsorption of dehydrogenated species which was the intermediate for formation of coke. Since Sn addition broke the Pt ensemble into the smaller metal clusters; consequently, the coke and hydrogenolysis reactions which favored to occur on large metal cluster were inhibited (Passos *et al.*, 1998). Furthermore, as shown in Table 4.4, the predominant aromatics products on bi- and trimetallic catalysts were C8-aromatics (EB and OX) with the small amount of benzene and toluene which are undesired products from hydrogenolysis reaction. Therefore, the addition of promoted metal caused a decrease in the hydrogenolysis products and increase in C8-aromatics products. Additionally, from previous studies, it was believed that tin decreased the hydrogenolysis reaction by the electronic effect since some electrons of tin were transferred to Pt when PtSn alloy phase was formed. Consequently, C-C bond hydrogenolysis does not occur because the hydrocarbon cannot be strongly adsorbed on the catalyst surface (Trakarnroek *et al.*, 2007). Not only was the hydrogenolysis reaction decreased by the electronic effect, but also the formation of OX molecules was also enhanced
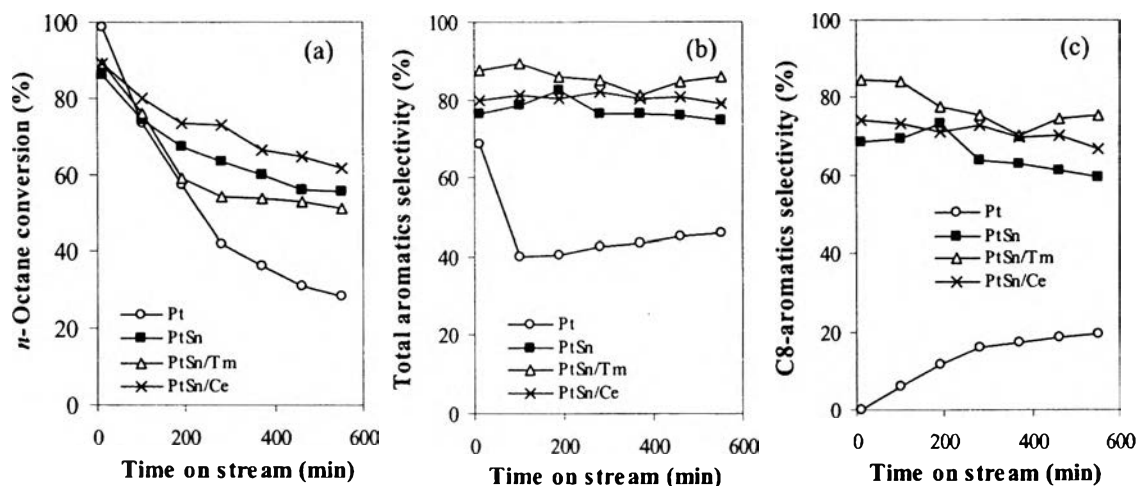
Figure 4.3 The variations of (a) *n*-octane conversion (b) total aromatics selectivity and (c) C8-aromatics selectivity vs. time on stream under clean *n*-octane feed over Pt/KL, PtSn/KL, and PtSn/RE/KL catalysts. Reaction conditions: WHSV = 5h^{-1}; H$_2$/HC molar ratio = 6; temperature = 500°C; pressure = 1 atm

as shown in Table 4.4. Westfall *et al.* (1976) and Lee *et al.* (1993) informed that the molar ratio of EB/OX may be an indirect index, indicating that electron density of Pt by the addition of Sn. Dehydrocyclization of *n*-octane produced EB and OX by a mechanism that involved the direct formation of a six-membered carbon ring (Davis *et al.*, 1969). The bond strength of primary hydrogen in –CH$_3$ is only greater than that of secondary hydrogen in –CH$_2$. Therefore, it was expected that the six-membered ring intermediate would lead to an almost equal amount of EB and OX (Meriaudeau *et al.*, 1997). However, Sn would alter the ability of Pt to rupture the C-H bond and favor the rupture of the weaker C-H bond of the secondary hydrogen of the –CH$_2$ groups over those of the primary hydrogen of the –CH$_3$ groups. Therefore, the EB/OX ratio was decreased when Sn was employed (Trakarnroek *et al.*, 2007). From Table 4.4, it was found that the EB/OX ratio of Pt was significantly high as a result of no electrons being transferred from Sn to Pt atoms. Contrarily, the bi- and trimetallic catalysts exhibited the EB/OX ratio less than unity while the Pt was greater than unity. The reason that gave the ratio of Pt/KL was greater than one because the critical size of the OX molecule is larger than that of EB which means the speed of transport through the pores is slower for OX than for EB. Hence, OX is

much easier to convert to smaller molecules such as benzene, toluene and methane by secondary hydrogenolysis. From Figure 4.3, the result showed that bi- and trimetallic catalysts obtained similar trends on both n-octane conversion and product selectivity. That means the addition of rare earths elements as the third metal did not significantly affect the catalytic activity and product selectivity in the case of sulfur-free feed.

4.2.2 Sulfur-containing Feed

As mentioned before, the high sensitivity of Pt/KL catalysts to sulfur is a major serious problem. They are much more sensitive to sulfur than conventional bifunctional reforming catalysts such as Pt/Al$_2$O$_3$ and PtRe/Al$_2$O$_3$ (Meriaudeau et al., 1997). In order to study the sulfur resistance of Pt/KL, PtSn/KL and PtSn/RE/KL catalysts, 2.5 ppm sulfur was added to the feed. The catalytic activity and C8-aromatics selectivity of sulfur-containing feed are obviously lower than clean feed. Figure 4.4 (a) shows the n-octane conversion versus time on stream. PtSn/RE/KL catalysts showed higher conversion than mono- and bimetallic catalysts, while C8-aromatics selectivity in Figure 4.4 (b) was not significantly different. In agreement with previous study, the presence of sulfur led to instantly weak bonding between metal and support, and then formation of Pt agglomeration and ultimately accelerating the seepage of Pt to the exterior surfaces which blocked the zeolite channel (McVicker et al., 1993, M.M.J Treacy, 1998). This induced larger Pt ensembles or clusters required for hydrogenolysis reaction in place of smaller ensembles being suitable for dehydrocyclization. This coincided with Table 4.4; it was found that hydrogenolysis products were increased for PtSn/KL and PtSn/RE/KL catalysts in sulfur-containing feed. Anyhow, Pt/KL did not correspond to the above mention. The reason could be because unpromoted Pt/KL was poisoned and rapidly deactivated which led to lower adsorption of hydrocarbons. Moreover, EB/OX ratio of Pt/KL exposing with sulfur as shown in Table 4.4 are much lower than that of clean feed while it did not have noticeable difference for bi- and trimetallic catalysts. Due to the fact that Pt inside the zeolite channel migrated to near pore mouth or outside the pore of zeolite, the probability to occur OX increased since there was no restricted diffusion out of the product inside the channel. In the case of bimetallic catalyst, sulfur

might break Pt-Sn alloy; which plays an important role for product selectivity, due to the fact that tin is an inert atom. Therefore, sulfur does not adsorb on tin but adsorbing with Pt instead leading to active particle growth (Garetto *et al.*, 1994, Borgna *et al.*, 2000). Consequently, PtSn/KL gave similar extent of *n*-octane conversion as the monometallic Pt/KL catalyst. This has to be further confirmed with characterization of spent catalyst by mild decoking. Nevertheless, trimetallic catalysts exhibited higher catalytic activity than mono- and bimetallic catalysts. From previous investigations, RE may help retard the rate of active site agglomeration. This inhibition can be due to two possible causes: (a) the RE may act as sulfur getter, or (b) the RE may prevent Pt growth by acting as sulfur anchoring sites for Pt. For these reasons, sulfur tolerance increases (Jacobs *et al.*, 1999, Jongpatiwut *et al.*, 2002).

In terms of aromatics product selectivity as shown in Figure 4.4 (b) and (c), it can be noticed that the selectivity of all catalysts in sulfur-containing feed is lower than clean feed. In the first 10 minutes, the product selectivity was not much distinct from sulfur-free feed. It would be due to the fact that there was partial alloy in the promoted catalyst remained at the first period of time. After that, sulfur started breaking the alloys. As a result, the data got from promoted catalysts were not much different from each other. Hence, RE did not help to improve the selectivity in sulfur-containing feed.
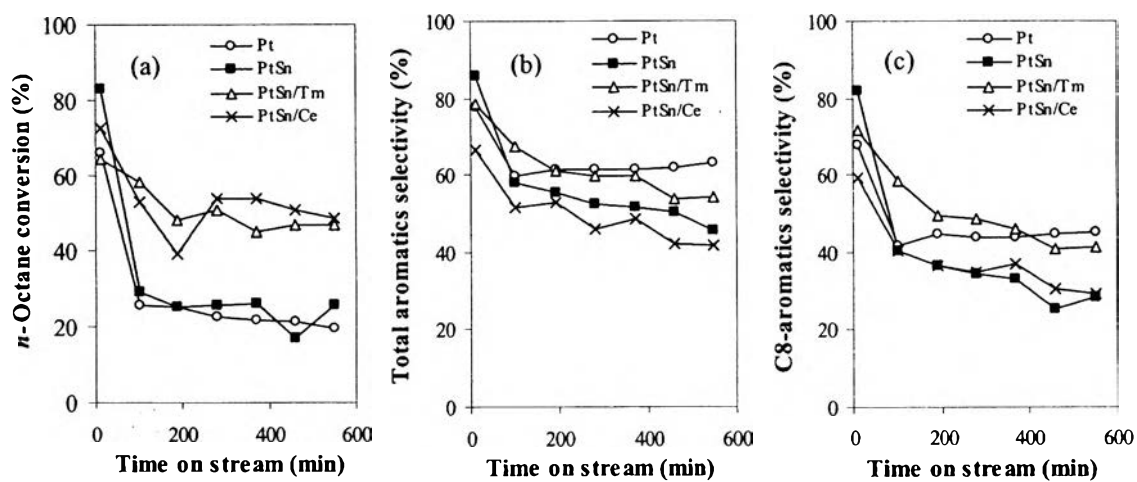
Figure 4.4 The variations of (a) n-octane conversion (b) total aromatics selectivity and (c) C8-aromatics selectivity vs. time on stream under 2.5 ppm sulfur-containing feed over Pt/KL, PtSn/KL, and PtSn/RE/KL catalysts. Reaction conditions: WHSV = $5h^{-1}$; H_2/HC molar ratio = 6; temperature = 500°C; pressure = 1 atm

Table 4.4 Properties of Pt/KL, CoPtSn/KL, and SeqPtSn/RE/KL catalysts tested for n-octane aromatization after 550 minutes time on stream under sulfur-free and 2.5 ppm sulfur-containing feeds; reaction conditions: WHSV = $5h^{-1}$; H_2/HC molar ratio = 6; temperature = 500°C; pressure = 1 atm.

Feed	Sulfur-free feed				Sulfur-containing feed			
Catalysts	Pt	CoPtSn	SeqPtSn/Tm	SeqPtSn/Ce	Pt	CoPtSn	SeqPtSn/Tm	SeqPtSn/Ce
Conversion (%)	24.5	56.1	51.3	61.8	19.4	25.8	46.7	48.6
Product distribution (%)								
C1-C5	22.9	7.1	1.6	5.1	10.5	20.2	25.9	38.5
Total enes (C6-C8enes)	30.7	16.9	12.4	13.9	26.3	34.4	19.8	19.9
Total aromatics	46.4	76.1	86.0	80.9	63.2	45.4	54.3	41.6
Total aromatics (%)								
Benzene	16.7	4.1	0.04	3.1	0.1	0.1	2.4	2.8
Toluene	6.9	10.8	10.0	7.5	17.7	17.0	10.8	9.4
C8-aromatics	22.8	61.2	75.6	70.3	44.9	28.3	41.1	29.4
EB	14.9	25.8	32.4	27.6	19.8	13.2	21.1	13.9
m-.p-Xylene	1.6	1.7	0.0	1.6	0.0	0.0	0.0	1.9
o-Xylene	6.3	33.8	43.2	41.0	25.0	15.0	20.0	13.6
EB/OX ratio	2.35	0.76	0.75	0.67	0.79	0.88	1.05	1.02
Hydrogenolysis products	46.5	21.9	12.0	15.8	28.8	37.3	39.1	50.7

4.3 Characterization of Spent Catalysts

TEM images of particle size distribution obtained by TEM of the Pt, PtSn, and PtSn/RE catalysts after running of reaction at 550 minutes are shown in Figure 4.5.
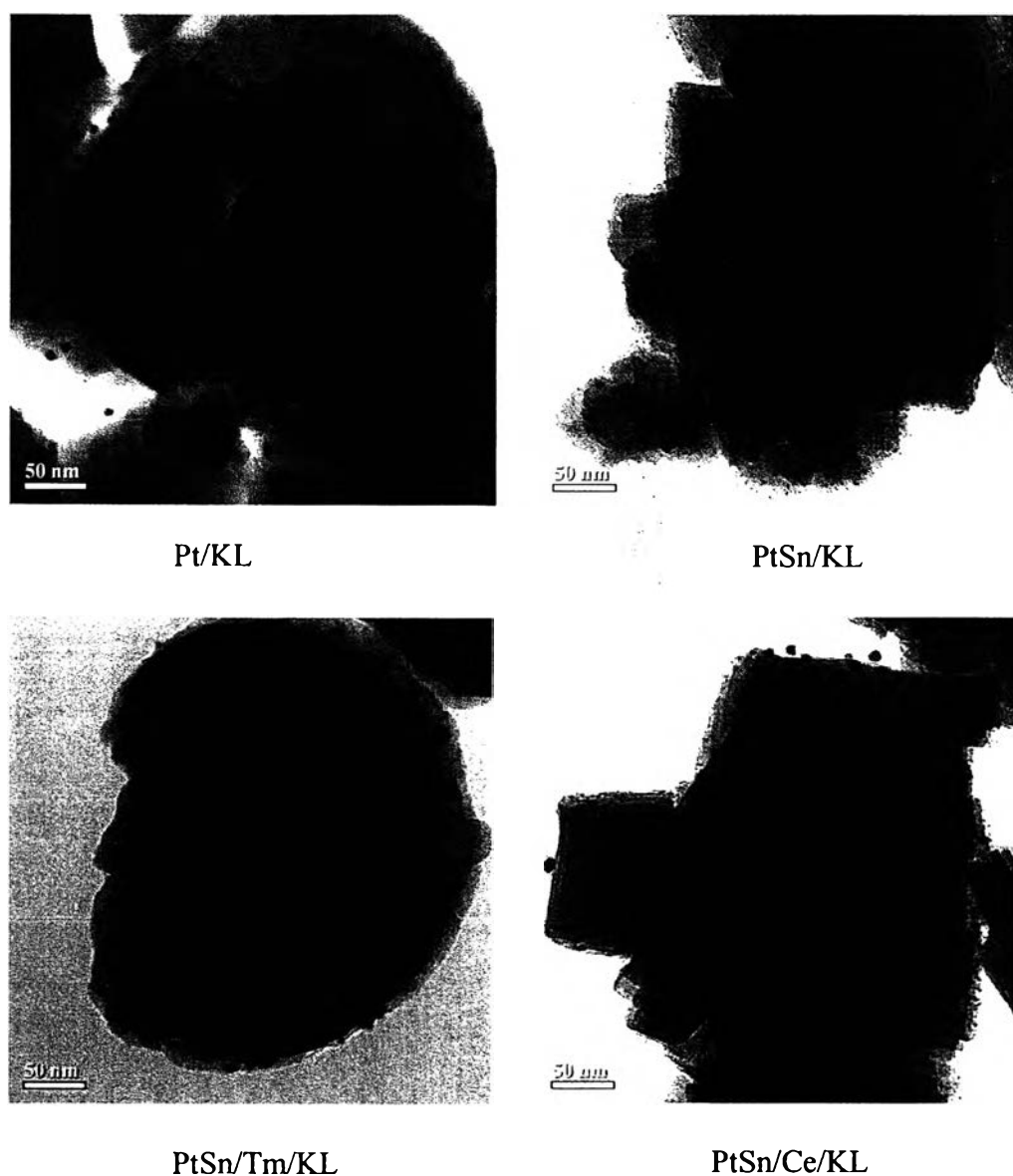

Pt/KL   PtSn/KL

PtSn/Tm/KL   PtSn/Ce/KL

Figure 4.5 TEM images of particle size distribution obtained by TEM of the spent Pt/KL, PtSn/KL, and PtSn/RE/KL catalysts

It was clearly seen that the particle size of spent catalysts was bigger than fresh ones. The reason of this could be because sulfur might induce metal particle size growth and resulted in lower metal dispersion which caused lower catalytic activity and C8-aromatics selectivity in Figure 4.4 (McVicker *et al.*, 1992). Although, TEM images could not indicate the existence of the metal inside the zeolite channel as mentioned before, the performance on both *n*-octane conversion and C8-aromatics selectivity for Pt/KL and PtSn/KL catalysts in this experiment agreed with previous investigations (Jongpatiwut *et. al.*, 2005, Trakarnroek, 2007) and was evident the presence of very fine particles inside the zeolite channel.

The spent catalysts were also characterized by TPO to quantify the amount of carbon deposited on the catalysts during the reaction in terms of percent weight of carbon. The coke formation obtained after reaction with feeds containing sulfur-free and sulfur-containing over Pt/KL, PtSn/KL, and PtSn/RE/KL catalysts are illustrated in Table 4.5.

Table 4.5 TPO analysis of spent Pt/KL, PtSn/KL, and PtSn/RE/KL catalysts under clean and 2.5 ppm sulfur-containing feed

Catalysts	Coke deposited after reaction 550 minutes TOS (wt%) Sulfur-free feed	Coke deposited after reaction 550 minutes TOS (wt%) 2.5 ppm Sulfur-containing feed
Pt/KL	2.9	1.1
PtSn/KL	2.1	1.8
PtSn/Tm/KL	1.3	1.7
PtSn/Ce/KL	2.0	2.1

In the case of non-sulfided samples, the monometallic Pt/KL catalyst was more deactivated by coke than bimetallic PtSn/KL and trimetallic PtSn/RE/KL catalysts. This agrees with the catalytic activity of clean feed in Figure 4.3 (a). Pt/KL rapidly deactivated by coke plugging inside the pore of KL zeolite because of the restricted diffusion out of the pore of C8-aromatic products (EB and OX) (Jongpatiwut *et al.*, 2005). Contrarily, Sn-promoted on the catalysts have less amount of coke due to the fact that tin decreased the number of contiguous platinum atoms and then
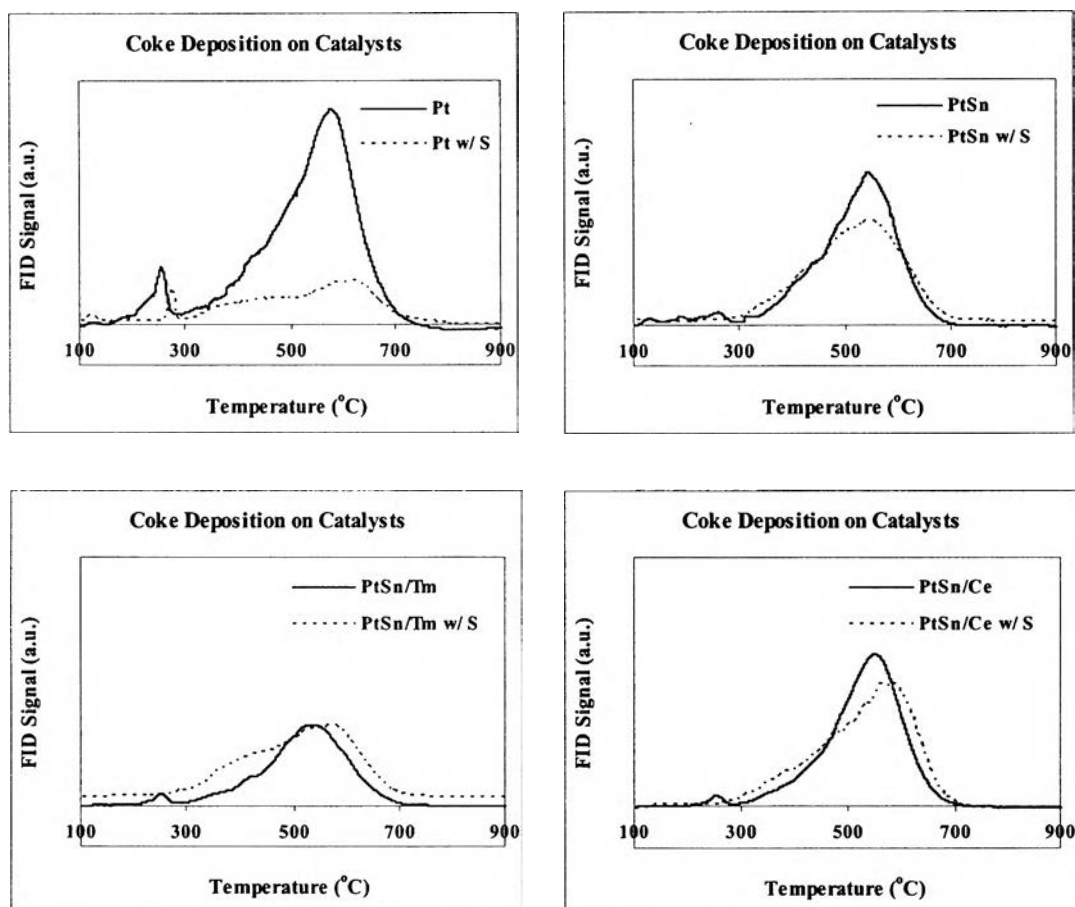
Figure 4.6 TPO profiles of spent Pt/KL, PtSn/KL, and PtSn/RE/KL catalysts under clean and sulfur-containing feeds

the multipoint adsorption of hydrocarbon molecules on the surface is hampered. Consequently, coke formation can be reduced (Paal *et al.*, 1997). However, coke formation in Table 4.5 was regarded as there was no significant change in carbon remained on the PtSn/KL and PtSnRE/KL catalysts for both clean and sulfur-containing feeds. While activity profiles of catalyst with sulfur-containing feed in Figure 4.4 (a) remarkably dropped as compared with those of clean feed in Figure 4.3 (a). That means the quantity of coke deposition in promoted catalysts was not affected by the presence of sulfur. From Figure 4.6, the peaks occurred at low temperature were corresponded to TEM images indicating some Pt particles outside the pore of zeolite. Therefore, coke deposited on these clusters was firstly burned out at low temperature. The amount of Pt at exterior zeolite channel for clean feed exhib-

ited higher than that of sulfur-containing feed. Also, Pt/KL showed the highest quantity of these clusters. Presumably, external Pt was poisoned by adsorbing with sulfur. It quickly deactivated, then Pt could not adsorb hydrocarbons which are coke precursors. As a result, the coke deposition peaks for external Pt in sulfur-exposing feed were lower than clean feed.

To prove that sulfur would segregate Pt-Sn and Pt-RE alloys, the spent catalysts were characterized by TPR after mild decoking at 350°C for 30 minutes. From Figure 4.7, there are three main peaks which correspond to Pt phase, metal interaction phase, and RE and Sn phase, respectively. The result displayed that TPR profiles showed the Pt-Sn interaction for the catalysts spent with sulfur-free feed but no Pt-Sn signal was observed on the spent catalysts with sulfur-containing feed. This demonstrates that the presence of sulfur induced the rupture of Pt-Sn alloy resulted in lower C8-aromatics selectivity which is shown in Figure 4.4 (c).
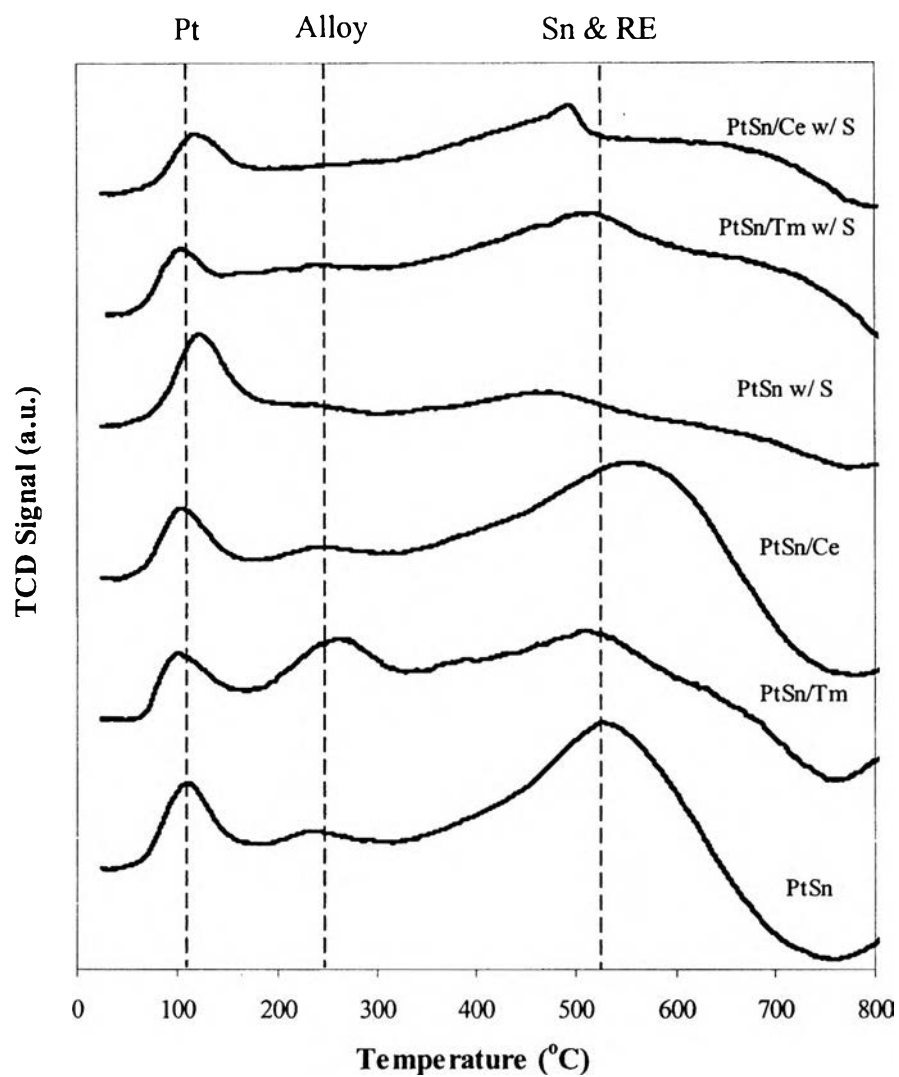
Figure 4.7 TPR profiles of the spent PtSn/KL and PtSn/RE/KL catalysts under clean and 2.5 ppm sulfur-containing feed after mild decoking at 350°C for 30 minutes